9th International Conference on Fracture Mechanics of Concrete and Concrete Structures
FraMCoS-9
V. Saouma, J. Bolander and E. Landis (Eds)
DOI 10.21012/FC9.145

STRAIN LOCALIZATION ANALYSIS OF AN ELASTIC-PLASTIC MODEL FOR HIGH PERFORMANCE FIBER REINFORCED CEMENTITIOUS COMPOSITES

MARTA MILETIĆ[*] AND DUNJA PERIĆ[†]

[*]Kansas State University
Manhattan, KS USA
e-mail: mmiletic@ksu.edu

[†]Kansas State University
Manhattan, KS USA
e-mail: peric@ksu.edu

Key words: High Performance Fiber Reinforced Cementitious Composites, Strain Localization, Exponential Drucker-Prager Model, Hyperbolic Drucker-Prager Model

Abstract: The main goal of this study was to develop and implement a combined analytical-numerical algorithm that can capture a stress-strain response and onset of strain localization in elastic-plastic fiber-reinforced cementitious composites. Multi-directional fibers are embedded into a matrix and the resulting composite is described by different non-linear, non-associated Drucker-Prager hardening plasticity models. The corresponding macroscopic tangent stiffness moduli tensor of the fiber reinforced composite is derived by consistently homogenizing the contribution of fibers in a representative volume element (RVE). Several actual uniaxial tension tests on non-reinforced cementitious composite as well as on the High Performance Fiber Reinforced Cementitious Composites (HPFRCC) were modelled. It was found that the presence of fibers delayed the inception of strain localization in all uniaxial tension tests on the HPFRCC as compared to the plain mortar. However, the onset of strain localization always coincided with yielding, thus indicating a slight fiber induced increase in the yield stress. More importantly, the results indicate that a significant increase in the peak load that is exhibited by HPFRCC is due to a distributed cracking that causes a global level hardening culminating in the significantly increased peak loads. Furthermore, the results also indicate that presence of fibers did not have any effect on the orientation and mode of accompanying deformation bands.

1 INTRODUCTION

Due to concrete's low ratio between its cost and its compressive strength, it is currently the most widely used construction material. Perhaps the main disadvantage of the concrete is its low tensile strength and limited tensile strain capacity, which are likely to produce detrimental effects.

For example, the present day concrete structures are often exposed to extreme loads, such as earthquakes, tsunamis, floods, fires, and large-scale unplanned events, which could lead to catastrophic failures that result in loss of human life and property damage. Low tensile strength of concrete and its limited tensile strain capacity are traditionally resolved by adding reinforcing steel, but research has shown that steel fibers could replace some of the reinforcing steel. Therefore, short discontinuous fibers with high tensile strength have been added to concrete mixes to improve their tensile strength and tensile strain capacities, thus directly

improving the resilience, toughness, and durability of concrete structures. The resulting material is known as fiber-reinforced concrete (FRC). Furthermore, a combination of proper fiber geometry with specifically tailored cementitious matrix whereby enhanced bond properties between the fibers and matrix are achieved leads to a strain-hardening behavior that turns the traditionally brittle material into a highly ductile material. This type of FRC is called high performance fiber-reinforced cementitious composite (HPFRCC) (Namaan and Reinhardt [1]).

HPFRCC has a high potential for achieving significant gains in engineering performance and economy, but it has not yet found its way into engineering practice. One of the main reasons for this may be the absence of computational models that would allow engineers to incorporate HPFRCC structural elements into their designs. Interest in HPFRCC is evident from the upsurge of related research activities in the last 15 years, most of which has been of experimental nature. A significant research related to the development of analytical models and numerical tools, as well as design procedures is needed for an accelerated uptake in the engineering practice. Although it appears that the main contribution of fibers, particularly in tension, occurs after the inception of strain localization a logical first step in the complete characterization of fiber effects is to conduct a rigorous analysis that can detect the onset of strain localization (OSL). To this end, the main goal of this study was to numerically capture a stress-strain response and predict the inception of strain localization in elastic-plastic HPFRCC.

Strain localization is a ubiquitous feature of elastic-plastic materials that signifies an inception of narrow zones, also known as deformation bands, within which large strains develop while little or no strain occurs outside of these zones. Thus, a strain localization can be characterized by a jump in strain rate across the boundary of a deformation or localization band. It is because the strain localization is followed by a softening response, typically leading to a catastrophic collapse of materials and structures that it is an important failure precursor. Consequently, a diagnostic strain localization analysis affords an improved characterization of the effect of fibers on the failure initiation by providing stress and strain levels at the inception of strain localization as well as orientations of accompanying discontinuities and corresponding strain localization modes. Ultimately, a diagnostic strain localization analysis supplies a quantitative measure of the fiber contribution towards an increased resilience of these important civil infrastructure materials.

Several researches have investigated the OSL in a plain non-reinforced concrete, such as Pietruszczak and Xu [2], Salari et al. [3], and Beizaee [4]. However, to the best knowledge of authors no previous significant attempts have been made towards conducting a diagnostic strain localization analysis in high performance fiber-reinforced cementitious composites. This study focused on HPFRCC, which was modeled by embedding multidirectional fibers into a matrix. The resulting composite was described by different two-invariant Drucker-Prager hardening plasticity models, including a hyperbolic Drucker-Prager (HDP), and an exponential Drucker-Prager (EDP) plasticity models with isotropic hardening. In addition, in order to investigate the effect of hardening type on the inception of strain localization, two types of isotropic hardening laws were used: linear and nonlinear hardening. Furthermore, a simple volume-based homogenization procedure was used to derive the corresponding macroscopic tangent stiffness moduli tensor of the fiber-reinforced composite. Actual uniaxial tension (UT) tests on non-reinforced mortar and on the HPFRCC were modelled.

2 FIBER CONTRIBUTION

The cubically shaped representative volume element (RVE) is shown in Figure 1. The side length of the RVE corresponds to two times the length of a fiber $L_{f.}$ Fibers have isotropic distribution throughout the RVE. It was assumed that fibers have a cylindrical shape with a diameter d_f, length L_f, and the aspect

(length to diameter) ratio η_f. Thus, a macroscopic tangent stiffness moduli tensor of the composite was developed by consistently homogenizing the contribution of fibers in the RVE (Miletić and Perić [5]).

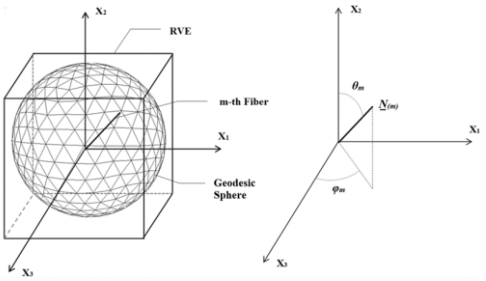

Figure 1: Distribution of fibers in the cubical RVE.

Volumetric fiber content χ_f was expressed as the ratio between the volume of fibers and the volume of the cubical RVE as follows

$$\chi_f = \frac{V_f}{V} = \frac{n_f \pi}{32\eta_f^2} \tag{1}$$

where V_f is the volume of fibers contained in RVE, V is the volume of the RVE, and n_f is the total number of fibers in the RVE.

Furthermore, a direction of a fiber is defined by its unit vector N_m. Therefore, for any fiber m, the components of the unit normal along the coordinate axes x_1, x_2, and x_3 are given by:

$$\begin{aligned} N_{1(m)} &= \sin\theta_m \sin\varphi_m \\ N_{2(m)} &= \cos\theta_m \\ N_{3(m)} &= \sin\theta_m \cos\varphi_m \end{aligned} \tag{2}$$

where angles θ_m and φ_m are shown in Figure 1.

The elastic contribution of fibers to the three-dimensional elastic stiffness moduli tensor $D^e_{ijkl,f}$ is given by:

$$D^e_{ijkl,f} = \frac{E_f}{n_f} \sum_{m=1}^{n_f} N_{i(m)} N_{j(m)} N_{k(m)} N_{l(m)} \tag{3}$$

where E_f is simply the elastic modulus of a fiber and m is the summation index.

3 TANGENT STIFFNESS MODULI TENSOR

The cementitious composite was assumed to be an elastic-plastic material experiencing an infinitesimal strain and obeying a general non-associative flow rule. Normal components of stress and strain tensors are positive in tension. The macroscopic stress-strain relationship for plastic loading is given by

$$\dot{\sigma}_{ij} = D^e_{ijkl}(\dot{\varepsilon}_{kl} - \dot{\varepsilon}^p_{kl}) \tag{4}$$

where $\dot{\sigma}_{ij}$, $\dot{\varepsilon}_{ij}$, and $\dot{\varepsilon}^p_{ij}$ are rates of the Cauchy stress tensor, infinitesimal strain tensor, and plastic strain tensor, respectively. D^e_{ijkl} is the corresponding elastic stiffness moduli tensor of the homogenized equivalent isotropic material. Thus, the elastic stiffness moduli tensor of the composite is defined as a weighted sum of the elastic stiffness moduli tensors of the matrix and of fibers given by

$$\begin{aligned} D^e_{ijkl} &= (1-\chi_f) D^e_{ijkl,m} + \chi_f D^e_{ijkl,f} \\ &= \mu(\delta_{ik}\delta_{jl} + \delta_{jk}\delta_{il}) + \lambda\delta_{ij}\delta_{kl} \end{aligned} \tag{5}$$

where $D^e_{ijkl,f}$ was given in Eq. (3), while an elastic stiffness moduli tensor of the matrix is given by

$$D^e_{ijkl,m} = \mu_m(\delta_{ik}\delta_{jl} + \delta_{jk}\delta_{il}) + \lambda_m\delta_{ij}\delta_{kl} \tag{6}$$

and δ_{ij} is Kronecker delta, μ_m and λ_m are Lamé's constants of the matrix, and μ and λ are Lamé's constants of the composite.

4 CONDITIONS FOR ONSET OF STRAIN LOCALIZATION

First, it is important to note that the diagnostic strain localization analysis was performed on the constitutive level herein. Thus, the inception of strain localization may be considered as a loss of stability of the constitutive relation governing the homogeneous deformation. Furthermore, a constitutive level response is not valid after the inception of strain localization.

The assumption was made that a weak discontinuity forms across a singular surface Γ with continuing loading, thus resulting in the

following expression for a jump in strain rate across the singular surface Γ (Runesson at al. [6])

$$\left[\dot{\varepsilon}_{ij}\right] = \frac{1}{2}\left(z_i n_j + z_j n_i\right) \tag{7}$$

where n_i is a unit vector, which is perpendicular to the characteristic surface Γ while z_i is the eigenvector corresponding to the relevant eigen-problem, as discussed below. It is assumed that material on both sides of the surface Γ responds plastically.

Furthermore, imposing the equilibrium along the singular surface and combining this condition with Eqn (7) leads to the classical bifurcation criterion (Rudnicki and Rice [7]), given by

$$Q_{ik} z_k = n_i D_{ijkl} n_l z_k = 0 \tag{8}$$

where Q_{ik} is an acoustic tensor, also known as a characteristic tangent stiffness tensor.

In order to solve for the critical amount of hardening necessary for the OSL, the following eigenvalue problem (EVP) was considered

$$Q_{ik} z_k^{(i)} = \lambda^{(i)} Q_{ik}^e z_k^{(i)}, \; i = 1,2 \tag{9}$$

Nontrivial solutions of the EVP are possible only when an acoustic tensor Q_{ik} is singular. Furthermore, only two eigenvalues are present in plane stress and plane strain states. One eigenvalue corresponds to elastic and the other one to plastic loading. By setting the plastic eigenvalue equal to zero, a hardening modulus $H(n_i)$ was obtained. Finally, the critical amount of hardening necessary for the OSL was obtained by solving the following constrained optimization problem

$$H_{cr} = \max_n H(n_i) \text{ where } n_i n_i = 1 \tag{10}$$

Analytical solutions for H_{cr} and corresponding strain localization directions for plane stress and plain strain were given by Runesson et al. [6]. Furthermore, the mode of shear band is defined by the jump in the volumetric strain rate, obtained from Eq. (7) as:

$$\left[\dot{\varepsilon}_v\right] = z_i n_i = \left|z_i\right| \cos\gamma \tag{11}$$

where γ is a mode angle or an angle between an eigenvector and a unit vector perpendicular to a deformation band defining the mode of strain localization.

5 APPLICATION TO DRUCKER-PRAGER MODELS

As mentioned previously, two types of two-invariant Drucker-Prager models were used in this study: HDP and EDP models (ABAQUS [8]).

The HDP model is a continuous combination of the linear Drucker Prager model at high confining stress and Rankine's maximum tensile stress criterion. The corresponding yield (F) and plastic potential (G) functions are given by

$$F(\sigma,\kappa) = \sqrt{(d'_0 - p_{t0}\tan\beta)^2 + q^2} - p\tan\beta - d'$$

$$G(\sigma) = \sqrt{(\epsilon\sigma_0\tan\psi)^2 + q^2} - p\tan\psi \tag{12}$$

where p and q are stress tensor invariants defined as

$$p = -\frac{1}{3}\sigma_{kk}, \; q = \left(\frac{3}{2}s_{ij}s_{ij}\right)^{\frac{1}{2}} \tag{13}$$

and s_{ij} is a stress deviator tensor. Parameter p_{t0} represents an initial hydrostatic tensile strength of a material, d' is a hardening parameter, d_0' is an initial value of d', and β corresponds to a friction angle measured at a high confining pressure. Furthermore, ϵ is a parameter referred to as an eccentricity. It defines the rate at which the function G approaches its asymptote, and σ_0 is an initial yield stress.

The yield function of the EDP model is given by

$$F = aq^b - p - p_{t0} \tag{14}$$

where a and b are material parameters, which are independent of plastic deformation. The plastic potential function G is the same as the one used by the HDP model.

Once the solution for the critical hardening modulus is obtained, detection of the OSL can be performed by comparing values of the actual and critical hardening moduli. Actual

hardening modulus H_{act} is obtained by numerical differentiation of the actual stress-plastic strain response obtained from Abaqus (ABAQUS [8]). Inception of strain localization occurs when the actual hardening modulus is equal to the critical hardening modulus.

Drucker-Prager models were calibrated based on UT, uniaxial compression (UC), and conventional triaxial compression (CTC) experiments, which were carried out at confining pressures of 41 and 52 MPa. The experiments were performed on plain mortar and on HPFRCC (Sirijaroonchai [9]). The resulting material parameters are shown in Table 1.

Table 1: Example of the construction of one table

Property	Mortar	HPFRC 1.0%	HPFRC 1.5%	HPFRC 2.0%
E (MPa)	26586	26655.5	26694.4	26717.1
v	0.2	0.2007	0.2011	0.2014
β (^{o})	27.57	30.79	30.87	29.94
d (MPa)	37.27	34.26	34.43	35.72
a	0.0004	0.00073	0.00074	0.00065
b	2.8	2.65	2.64	2.67
p_t (MPa)	0.27	0.38	0.4	0.41
ψ (^{o})	21.80	15.12	12.95	11.31

Although experimental data are available for four volumetric fiber contents (0%, 1%, 1.5%, and 2%), the data for only three fiber contents (0%, 1%, and 2%) were used during the calibration procedure.

Isotropic hardening was used in all models. The hardening function was prescribed in a tabular form based on the experimental data obtained from UT tests. For non-reinforced cementitious composites, the assumption was made that deviatoric stress at the onset of yielding coincided with the peak deviatoric stress in UT, thus resulting in no hardening.

6 RESULTS

Figures 2 and 3 depict the comparisons between the numerically predicted and experimentally observed responses in UT test for the HDP and EDP models, respectively.

Figures 2 and 3 show that addition of fibers to the mortar slightly increased the yield stress in UT while it more significantly increased the peak stress and tensile strain capacity. For example, for a volumetric fiber content of 0% the yield stress was approximately 0.77 MPa. However, for the volumetric fiber content of 1% the yield stress increased to approximately 1.1 MPa. More so, the peak stresses of HPRFCCs were at least four times higher than the peak stress of the plain cementitious composite. The predicted axial strain level at the OSL in the plain mortar coincided with the axial strain level at which a severe post peak drop in deviatoric stress began. On the contrary, the predicted OSL in fiber reinforced materials was followed by a significant hardening leading to significantly increased peak stresses as compared to the plain mortar. Thus, it appears that the principal mechanism of the delayed OSL in the UT tests was fiber-induced slight increase in the yield stress. Furthermore, the numerical predictions seem to indicate that OSL in plain mortar coincides with the formation of the major crack. On the contrary, the OSL in HPFRCC indicated the inception of distributed cracking that manifests itself in a global level hardening mechanism. Thus, the major crack development was delayed through the mechanism of fiber induced distributed cracking that requires a regularized finite element model for its computational capture. The latter is beyond the scope of this paper.

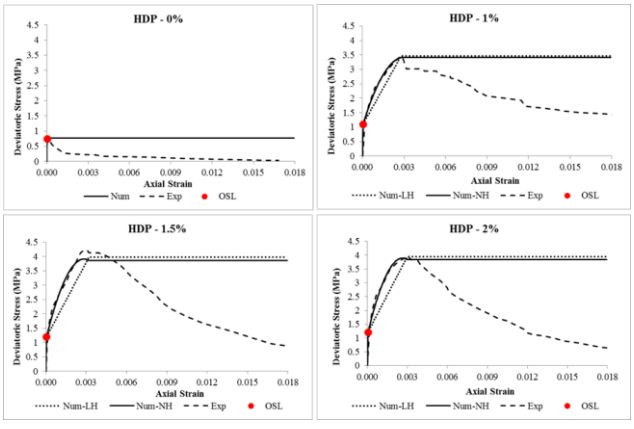

Figure 2: Experimentally observed and numerically predicted responses for HDP model with linear and nonlinear hardening (HPFRCC with volumetric fiber content of 0%, 1%, 1.5% and 2%).

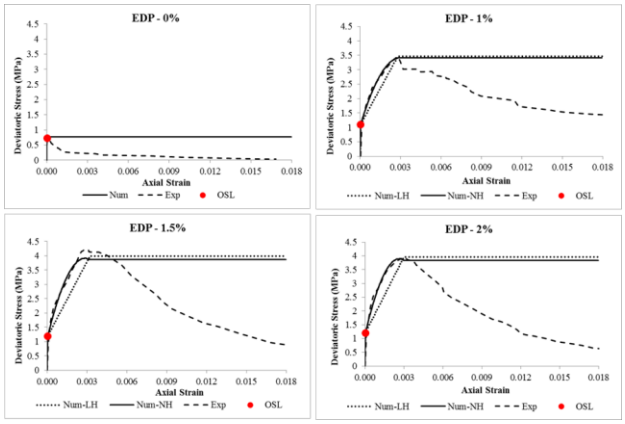

Figure 3: Experimentally observed and numerically predicted responses for EDP model with linear and nonlinear hardening (HPFRCC with χ_f of 0%, 1%, 1.5% and 2%).

Figure 4 shows axial strain values at the OSL for different volumetric fiber contents. The figure shows that the presence of fibers delayed the inception of strain localization in all UT tests. These findings were validated by two types of plasticity models for UT test.

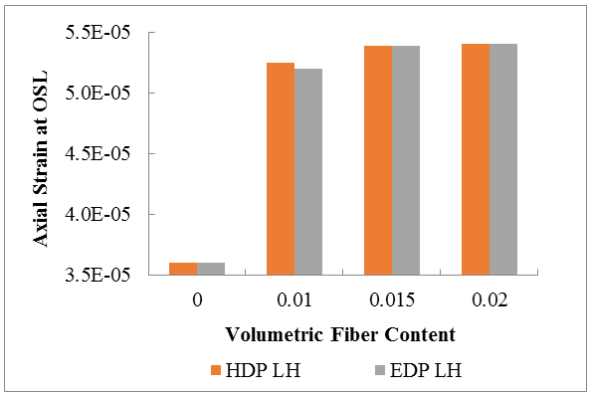

Figure 4: Axial strain at the OSL for χ_f for plane stress UT test.

Figure 5 shows the effect of hardening type on the inception of strain localization. Two types of hardening were considered: linear and nonlinear hardening rules. Results for the unreinforced cementitious composite in UT are not shown in Figure 5 because the composite was assumed to not experience any hardening during the UT test. As shown in the figure, the hardening type did not significantly affect the OSL in the UT tests.

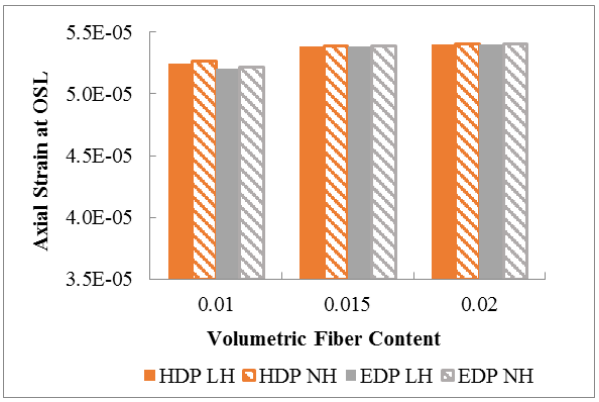

Figure 5: Axial strain at the OSL for various χ_f and different types of hardening for plane stress UT test.

Figure 6 summarizes values of the axial stresses at the OSL for various volumetric fiber contents and different types of hardening. It can be observed that the addition of fibers to the plain composite increased the level of axial stress at the OSL. Type of hardening had minor influence on the values of stress at the OSL in the UT test.

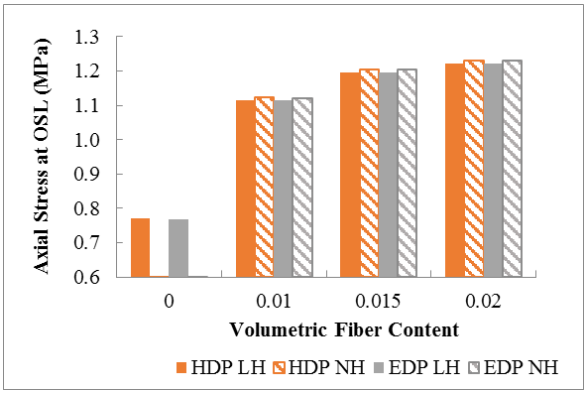

Figure 6: Axial stress at the OSL for various χ_f and different types of hardening for plane stress UT test.

Figure 7 shows orientation of the deformation bands. It is evident from Figure 7 that fibers did not affect the orientation of deformation bands in the UT tests at all. For each case, the orientation was 90°, implying that deformation bands were perpendicular to the direction of the major principal stress. Furthermore, fibers did not have any effect on the mode angle as well. Mode angles for each volumetric fiber contents remained equal to zero, thus signifying pure dilation bands.

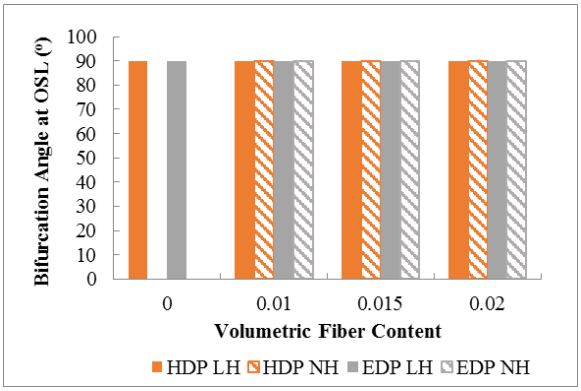

Figure 7: Critical bifurcation angle versus volumetric fiber content for UT test.

7 CONCLUSIONS

The main goal of this study was to perform computational modeling of strain localization in HPFRCC in order to quantify the effects of fibers on the OSL in UT in elastic-plastic cementitious composites.

To this end, a combined numerical-analytical algorithm that can capture a constitutive level stress-strain response and inception of strain localization in HPFRCC was developed and implemented. Predictions of the homogeneous stress-strain responses were successfully validated primarily against the experimental data for HPFRCC with volumetric fiber content of 1.5% from UT tests.

The inception of strain localization coincided closely with the onset of yielding in the plain and reinforced cementitious composites. However, the onset of yielding in HPFRCC was slightly delayed as compared to that in plain mortar. Based on the results of a rigorous strain localization analysis it is concluded that the enhanced performance of HPFRCC is achieved through a distributed cracking that appears to generate a global level hardening, thus leading to the increased peak loads.

Results also showed that fibers affected neither the critical bifurcation angle nor the mode of deformation band in the UT tests. Thus, deformation bands remained perpendicular to the principal stress direction in UT tests. Furthermore, they were all pure dilations bands, thus resembling the crack mode I in fracture mechanics.

REFERENCES

[1] Namaan, A.E., and Reinhardt, H.W. 1995. *High Performance Fiber Reinforced Cement Composites 2*, pp. 232-269.

[2] Pietruszczak, S., and Xu, G. 1995. Brittle response of concrete as a localization problema. *International Journal of Solids and Structures* 32(11):1517-1533.

[3] Salari, M. R., Saeb, S., Willam, K.J., Patchet, S. J., and Carrasco, R.C. 2004. A coupled elastoplastic damage model for geomaterials. *Computer Methods in Applied Mechanics and Engineering* 193:2652-2643.

[4] Baizae, S. 2013. Constitutive modeling and numerical implementation of brittle and ductile material behavior with the aid of inelastic XFEM and damage-plasticity models. *PhD thesis*. University of Houston, United States of America.

[5] Miletić, M. and Perić, D. 2015. Onset of Strain Localization in Fiber Reinforced Composites Subjected to Plane Stress Loading. In Chau, K. T. and Zhao, J. (Eds) *Bifurcation and Degradation of Geomaterials in the New Millennium, Proceedings of the 10th International Workshop on Bifurcation and Degradation in Geomaterials*. pp. 279-283.

[6] Runesson, K., Ottosen, N. S. and Perić, D. 1991. Discontinuous bifurcations of elastic-plastic solutions at plane stress and plane strain. *International Journal of Plasticity* 7: 99-121.

[7] Rudnicki, J.W., and Rice, J.R. 1975. Conditions for the localization of deformation in pressure-sensitive dilatant materials. *Journal of the Mechanics and Physics of Solids* 23: 371-394.

[8] ABAQUS. 2013. Version 6.13-1. *Dassault Systemes Simulia Corporation*. Providence, Rhode Island.

[9] K. Sirijaroonchai (2009). "A macro-scale plasticity model for high performance fiber reinforced cement composites." Ph.D. thesis, The University of Michigan, United States of America.